Molecular dynamics studies of melting and solid-state transitions of ammonium nitrate

Gustavo F. Velardez, Saman Alavi, and Donald L. Thompson
Department of Chemistry, Oklahoma State University, Stillwater, Oklahoma 74078

(Received 10 October 2003; accepted 23 February 2004)

Molecular dynamics simulations are used to calculate the melting point and some aspects of high-temperature solid-state phase transitions of ammonium nitrate (AN). The force field used in the simulations is that developed by Sorescu and Thompson [J. Phys. Chem. A **105**, 720 (2001)] to describe the solid-state properties of the low-temperature phase-V AN. Simulations at various temperatures were performed with this force field for a $4\times4\times5$ supercell of phase-II AN. The melting point of AN was determined from calculations on this supercell with voids introduced in the solid structure to eliminate superheating effects. The melting temperature was determined by calculating the density and the nitrogen–nitrogen radial distribution functions as functions of temperature. The melting point was predicted to be in the range 445 ± 10 K, in excellent agreement with the experimental value of 442 K. The computed temperature dependences of the density, diffusion, and viscosity coefficient for the liquid are in good agreement with experiment. Structural changes in the perfect crystal at various temperatures were also investigated. The ammonium ions in the phase-II structure are rotationally disordered at 400 K. At higher temperatures, beginning at 530 K, the nitrate ions are essentially rotationally unhindered. The density and radial distribution functions in this temperature range show that the AN solid is superheated. The rotational disorder is qualitatively similar to that observed in the experimental phase-II to phase-I solid-state transition.
 [DOI: 10.1063/1.1705573]

I. INTRODUCTION

Ammonium nitrate has a melting point of ~442 K at atmospheric pressure and a decomposition temperature at 463 K.[1] At normal pressures, AN exists in one of five crystalline phases.[2–11] These phases are designated with Roman numerals in the widely used system[12] where I is the phase stable at high temperatures, which then converts to phase II upon cooling, and so on. Projections of four of the AN phases (V, IV, II, and I) on the $a-b$ planes are illustrated in Fig. 1; phase III is not shown since traces of water are needed for its formation. Three-dimensional structures of the unit cells for these phases are given in Sorescu and Thompson.[13] The structures of these phases are closely related to one another and little change in the positions of the centers-of-mass of the ions is needed to interconvert these phases. As typical of some ammonium salts, orientational disorder (see below) in the crystal phases increases as temperature increases. There are eight AN molecules in the low-temperature phase-V orthorhombic unit cell ($Z=8$), which is stable between 0 and 255 K.[2,3] This phase (see Fig. 1) has a three-dimensional hydrogen-bond network between the ammonium and nitrate ions and the lengths of the O···H hydrogen bonds (between 1.916 and 1.987 Å), are the shortest among the solid-state AN phases. At 255 K phase V is transformed to the orthorhombic phase-IV with $Z=2$. In phase IV (see Fig. 1), the network of O···H hydrogen bonds in the unit cell forms a set of planes parallel to the (001) face.[4–7] Phase IV is stable up to 323 K. At this temperature phase-IV undergoes a transition to the tetragonal phase-II, which also has $Z=2$.[7] In this phase, the nitrates ions in alternating planes have rotated by $\pi/4$ and $-\pi/4$, respectively, relative to the orientation of the hydrogen-bonded planes of nitrates in phase-IV. The nitrate ions show static disorder between these two orientations. Two orientations, related by a $\pi/2$ rotation about the [001] direction, are also possible for the ammonium ions in phase-II. Due to the weak hydrogen-bonding, the two ammonium orientations are considered to be dynamically disordered.[7,10] This is illustrated by the circles around the ammonium ions in Fig. 1. At 398 K phase II is transformed to the cubic phase-I, Fig. 1, which has $Z=1$ with both the ammonium and nitrate ions dynamically disordered.[8–11] The x-ray diffraction pattern of phase I has been interpreted in terms of a ''12-orientation model'' for the nitrates.[10] However, neutron powder diffraction methods[9] and comparative Raman studies of phases IV, II, and I imply that the motion of the nitrate ions in phase I approaches free rotation.[11] Phase I is stable up to the melting point.

In an earlier study,[13] we computed structural and electronic properties by using density functional theory and the pseudopotential method for phases V to II, obtaining results in good agreement with the experimental data.[2–6] We developed a force field for phase V and used it in classical molecular dynamics (MD) calculations to evaluate variations of the lattice and elastic constants and changes in the radial distribution function (RDF) with temperature. Our interest here is to extend this work to simulations of the solid-to-liquid-phase transition and to investigate the II→I phase transition.

We begin the simulations with the experimental phase-II crystal structure. The main focus of this work is to simulate

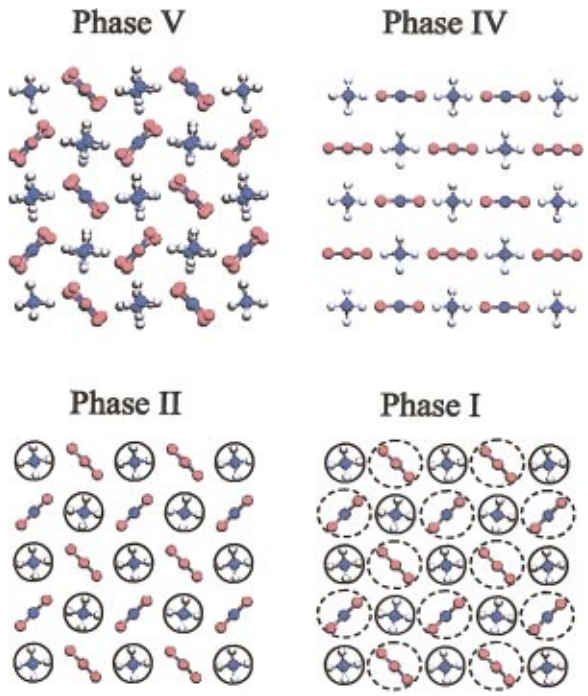

FIG. 1. (Color) An illustration of the basic features of the AN phases V, IV, II, and I projected onto the $a-b$ plane of the supercell. The rotational freedom of the ions in the higher-energy phases is illustrated by the circles that crudely represent the paths of the oxygen and hydrogen atoms as the nitrate and ammonium ions rotate. Phase III is not shown because it contains water.

the solid-to-liquid transition; specifically we wish to determine how accurately our model predicts the melting point of AN. We initiated the simulations of melting with the phase II structure rather than that for phase I, which is the solid phase at which the melting transition occurs, because the coordinates for the ill-defined phase I are not available. The melting transition was still properly predicted, although we began the simulation with the phase II crystal structure. Simulating crystalline phase changes is difficult because they often involve subtle variations in the geometry and unit cell parameters.[14] Although realistic theoretical descriptions require accurate intermolecular potentials, in particular, the angular dependence of hydrogen bonding in the case of AN, the results of the present study show that some basic changes in the solid are qualitatively predicted by the present approximate model potential.

We have used the Sorescu–Thompson[13] potential in the simulations. The melting point was determined from simulations of perfect and imperfect (i.e., with voids) phase-II crystals at various temperatures. The melting transition has been characterized by the temperature dependence of the density and radial distribution functions (RDFs). The density, diffusion coefficients, and viscosity have also been calculated for liquid AN over the narrow temperature range 442–462 K for which the liquid is stable at atmospheric pressure and the calculated density and viscosity values are compared with to experimental data.

A free energy barrier to the formation of a solid–liquid interface must be overcome in a direct MD simulation of the melting of a perfect crystalline solid.[15,16] As a result, superheating can occur in perfect crystals and direct MD simulations of perfect crystals lead to calculated melting points that are typically 20%–30% larger than the experimental values.[17,18] Various practical methods have been developed to bypass this problem. The method used here is to compute the melting points by simulating imperfect crystals. The free energy barrier to the formation of a solid–liquid interface can be lowered by introducing imperfections, such as voids, in the crystal.[19–21] Each void is formed by removing a single AN molecular unit from the supercell. Upon heating or equilibration, the local structure around a void is rapidly disordered and forms a pocket of liquidlike structure within the solid. However, if the number of voids is sufficiently large (typically greater than 10% of the total number of molecules in the supercell), the crystal structure breaks down even at low temperatures and the melting transition is no longer observable.

We have recently reported studies of melting of nitromethane[22] and ammonium dinitramide[23] using this approach. These studies support the validity of this method for accurate predictions of melting in relatively complex solids. Further details about the method used in this work and other simulation methods for studying of melting are given in Refs. 22 and 23.

This paper is organized as follows: In Sec. II the force field for AN and MD simulation methods are discussed. In Sec. III the results of the MD calculations of melting and liquid-state properties of AN are presented. In Sec. IV we give an analysis of the changes in orientational disorder and rotational freedom of the ammonium and nitrate ions seen in the phase II structure as the temperature is increased. Changes that correspond to the II→I transition are presented in Sec. IV. A summary and the conclusions are given in Sec. V.

II. METHODS

The force field for AN was obtained from the work of Sorescu and Thompson.[13] The intramolecular potential has the functional form,

$$V_{\text{intra}} = \sum_{\text{stretch}} \frac{1}{2} k_{ri} (r_i - r_i^0)^2 + \sum_{\text{bend}} \frac{1}{2} k_{\theta i} (\theta_i - \theta_i^0)^2 + \sum_{\text{torsion}} 2k_\Phi \sin^2 \Phi. \quad (1)$$

Harmonic functions with force constants k_r and k_θ describe the intramolecular bond stretching and angle bending force constants, respectively. The ''improper torsion'' potential with force constant k_Φ maintains the planarity of the nitrate group by restraining each O-atom to motion about the plane of the remaining $-NO_2$ part of each nitrate ion.

Sorescu and Thompson[13] described the intermolecular interactions with a sum of pairwise additive atom–atom 12-6 Lennard-Jones (LJ) potentials for the nonhydrogen-bonding interactions and a shorter ranged pairwise additive 12-10 hydrogen-bonding (HB) potential for hydrogen–oxygen interactions. Electrostatic (ES) interactions between point charges centered on the nuclei of the ions are also included in the intermolecular potential,

TABLE I. Intramolecular potential parameters.[a]

Bond	k_r (kJ·mol^{-1}·Å^{-1})	r^0 (Å)
N_1-O	3699.1769	1.028
N_2-H	3480.9346	1.264
Bond angle	k_θ (kJ/mol·rad^2)	θ^0 (deg)
$H-N_1-H$	327.8218	109.63
$O-N_2-O$	1092.3241	120.00
Dihedral	k_Φ (kJ·mol^{-1})	
$O-N_2-O-O$	794.2765	

[a]From Sorescu and Thompson, Ref. 13.

TABLE II. Intermolecular potential parameters.[a]

H-bond potential: Pair	A_{ij}^{H} (kJ/mol·Å)[b]	B_{ij}^{H} (kJ/mol·Å)[c]
O···H	1662.97	674.54
L-J 12-6 potential: Pair	A_{ij} (kJ/mol·Å)[b]	B_{ij} (kJ/mol·Å)[c]
H–H	2195.37	124.87
N–N	1904534.60	1508.90
O–O	1970959.87	2739.50
O–N	3735452.02	3484.43
N–H	100441.03	454.45

[a]From Sorescu and Thompson, Ref. 13.
[b]Reference 12.
[c]Reference 10.
[d]Reference 6.

$$V_{\text{inter}}=\sum_{i=1}^{N-1}\sum_{j>i}^{N}\{V_{ij}^{\text{LJ}}+V_{ij}^{\text{HB}}+V_{ij}^{\text{ES}}\}, \tag{2}$$

where

$$V_{ij}^{\text{LJ}}(r_{ij})=\frac{A_{ij}}{r_{ij}^{12}}-\frac{B_{ij}}{r_{ij}^{6}},$$

$$V_{ij}^{\text{HB}}(r_{ij})=\frac{A_{ij}^{\text{H}}}{r_{ij}^{12}}-\frac{B_{ij}^{\text{H}}}{r_{ij}^{10}},$$

and

$$V_{ij}^{\text{ES}}(r_{ij})=\frac{q_i q_j}{4\pi\varepsilon_0 r_{ij}}$$

and r_{ij} is the interatomic separations of pair i and j which carry electrostatic atom-centered charges q_i and q_j. The permittivity constant for vacuum is ε_0.

The values of the force constants used in the intramolecular potential were determined by fitting scaled *ab initio* MP2/6-31G(d,p)-level frequencies of gas phase NH_4^+ and NO_3^-. The electrostatic charges in Eq. (2) were originally determined by the fitting method of Breneman and Wiberg.[24] We also determined charges by using the restricted electrostatic potential (RESP) procedure of Bayly *et al.*[25] given in the AMBER 7 package.[25–27] The two sets of charges are basically identical. The values of the remaining intermolecular potential parameters are the same as those determined for ammonium dinitramide (ADN),[28] with the exception of the N···O and H···O intermolecular interactions which were refit to obtain the proper crystal structure for phase V ammonium nitrate. The values of the intramolecular potential parameters, intermolecular force constants and electrostatic monopole atomic charges are given in Tables I, II, and III, respectively.

Constant pressure (1 atm) and temperature (NPT) molecular dynamics simulations with isotropic volume variation for a $4\times4\times5$ supercell have been performed with the DL_POLY 2.12 molecular dynamics program.[29] The simulations use the Nosé–Hoover barostat algorithm[30,31] as implemented in the DL_POLY program with relaxation times for temperature and pressure in the barostat equal to 0.1 and 1.0 fs, respectively. The equations of motion were integrated using the Verlet leapfrog scheme.[32] A $4\times4\times5$ supercell was used as the initial configuration to give an approximately cubic simulation box: $22.88\times22.88\times24.66$ (in Å). All interatomic interactions in the simulation box were included along with interactions among nearest image sites within a cutoff distance of $R_{\text{cutoff}}=10.0$ Å. Long-range Coulombic interactions were calculated by using Ewald's method,[32,33] with a precision of 1×10^{-6}.

Each NPT simulation was equilibrated for 10 000 time steps and averages computed over the following 290 000 steps (one time step equals 0.5 fs). The input configuration corresponds to the experimental crystal structure of phase-II ammonium nitrate at 323 K,[7] a portion of which is shown in Fig. 2(a). Constant temperature and pressure simulations were performed over the range 323 K to 650 K at 1 atm. This approach, rather than ''heating simulations'' as we used in Ref. 22, allows the averaging of large amounts of data at each temperature (i.e., the averages are obtained for a large number of time steps) that gives much better convergence for the structural and thermodynamic quantities. The values of the temperature for the individual simulations have an uncertainty of ±10 K. For simulations at temperatures where a solid-to-liquid phase change occurs, the averages of properties were computed over the liquid-state portion of the trajectories, and in these cases, the simulation time was extended to ensure convergence of the liquid-state properties.

III. MELTING OF AMMONIUM NITRATE

Snapshots of the supercell of the phase-II solid at different temperatures are shown in Fig. 2. These snapshots are projections looking downwards on the $a-b$ plane of the supercell. The simulations at all temperatures were begun with

TABLE III. Calculated atomic charges for isolated NH_4^+ and NO_3^-.

Atom[a]	Charge[b]	Charge[c]
NH	−0.774701	−0.744
H	0.443675	0.443
NO	0.896259	0.898
O	−0.632086	−0.632

[a]NH is the nitrogen on ammonium and NO is the nitrogen on nitrate.
[b]From Sorescu and Thompson, Ref. 13.
[c]From RESP fit.

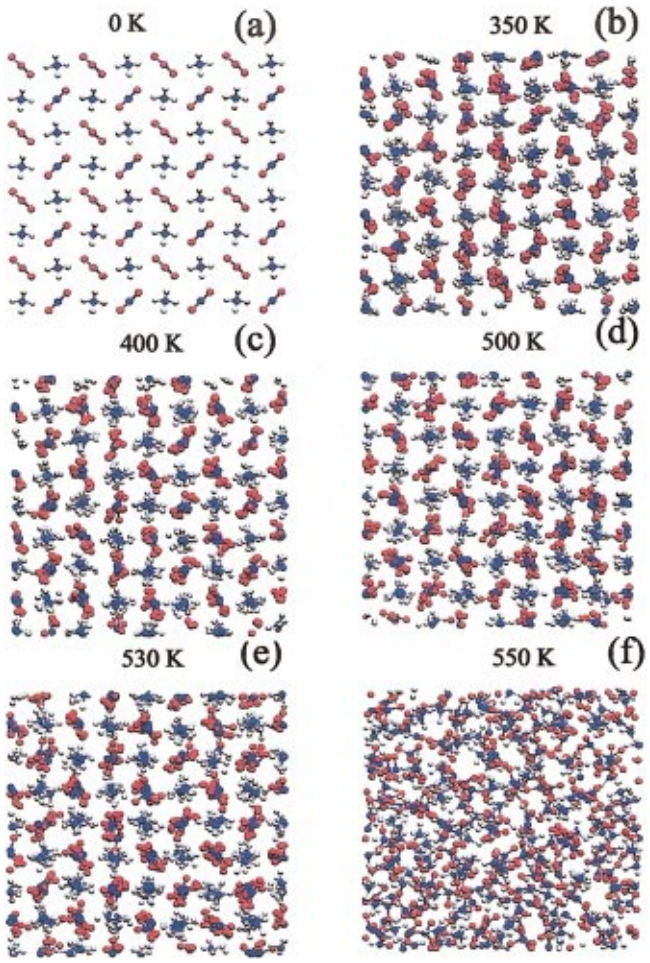

FIG. 2. (Color) Projection of the $4\times4\times5$ perfect crystal supercell in the $a-b$ plane at various temperatures (N-atoms: blue; O-atoms: red; H-atoms: gray). (a) Initial structure of a perfect AN solid phase II obtained from crystallographic data, used as input in the MD calculations. (b) A snapshot of the structure of solid AN at 350 K. The ammonium ions are rotationally disordered but translationally ordered at this temperature. (c)–(f) Snapshots of the structure of the supercell at the indicated temperatures. These results indicate that melting occurs between 545 K and 555 K, but based on density we predict the melting point to be 445 K for imperfect crystals.

a perfect crystal as the initial configuration. Figure 2(a) shows the perfect crystal structure for phase-II with the plane of the nitrate ions of adjacent rows oriented perpendicular to one another. Subsequent snapshots show the simulation cell after equilibration at higher temperatures. In Figs. 2(b)–2(e), which are snapshots at temperatures in the range of 350–530 K, the ammonium ions are rotationally disordered. The hydrogen atoms of the ammonium ions in successive layers of the supercell are randomly oriented. The nitrate ions generally retain the ordered orientations of the perfect crystal but undergo fairly large-amplitude motions about these original orientations. At 550 K the solid has melted and the ions are translationally free.

The first-order melting transition of a crystal phase is quantitatively characterized by discontinuous variation of some equilibrium and structural properties. In particular, the density, and RDFs show discontinuous variations at the melting point. We have calculated these properties for a $4\times4\times5$ supercell of AN to determine T_{mp}.

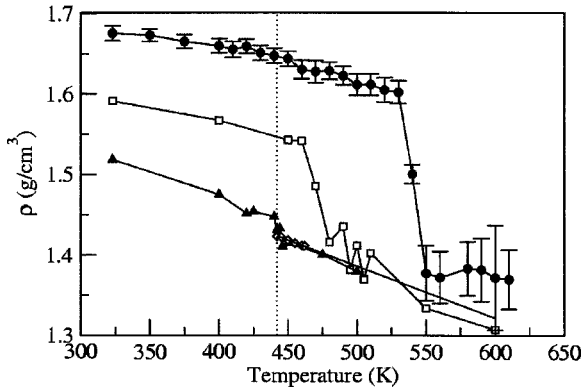

FIG. 3. (●) Average density of AN as a function of the temperature from the $4\times4\times5$ supercell simulation. The points are connected by straight lines for clarity. Based on these results, the melting point of the perfect crystal is predicted to be 540 K. (□) Average density for 8 voids, which predicts the melting point to be 475 K. (▲) Average density for 16 voids, which predicts the melting point to be 445 K. (◇) Density of liquid AN; the line is $\rho = 1.71 - 6.75\times10^{-4}\,T$, which was obtained by a least-squares fit to the points.

The variation of density with temperature for simulations starting from a $4\times4\times5$ supercell perfect crystal of phase-II AN is shown in Fig. 3, where the points (●) are connected by straight lines for clarity. The calculated density of phase-II AN at 350 K (1.643 g/cm^3) is in good agreement with the experimental value of 1.648 g/cm^3. A drop in the density corresponding to $\Delta\rho_{\mathrm{calc}}\approx0.2$ g/cm^3 is seen at 540 K, which corresponds to the calculated melting point. This temperature is ~1.22 times the experimental melting point of 442 K. The overestimation of T_{mp} is due to the superheating effect, which was discussed in the Introduction.[1,17,34] The harmonic bond stretching and angle bending terms in the force field for AN do not allow for chemical decomposition and so the high temperature simulations do not correspond to the real state of AN. Simulations for temperatures higher than 540 K give liquid AN as the final product. Densities calculated from direct liquid-state simulations (◇) for temperatures from the experimental value of T_{mp} to the decomposition temperature of liquid AN are shown in Fig. 3 for comparison. Note that the temperature dependence of the density calculated in the direct liquid simulations is consistent with that obtained from the melting runs which begin with a solid-state configuration, which is illustrated by the straight line that is drawn through both sets of points.

To eliminate superheating effects in the perfect crystal, calculations were performed on a $4\times4\times5$ supercell with eight and sixteen ion-pair voids. Two-molecule voids were created by removing a unit cell from the simulation supercell. The locations of the voids were uniformly distributed in the crystal. Sixteen ion-pair voids equals 10% of the total number of ion pairs (160) in the original ensemble. This is the upper limit to the number of voids, as determined by Agrawal *et al.*,[35] for which a melting transition can be simulated. The density as a function of temperature is shown for simulations of supercells with eight (□) and sixteen (▲) ion-pair voids in Fig. 3. The vertical dashed line indicates the experimental melting point. The computed melting point decreases with increasing number of voids and is $T\approx445$ K for

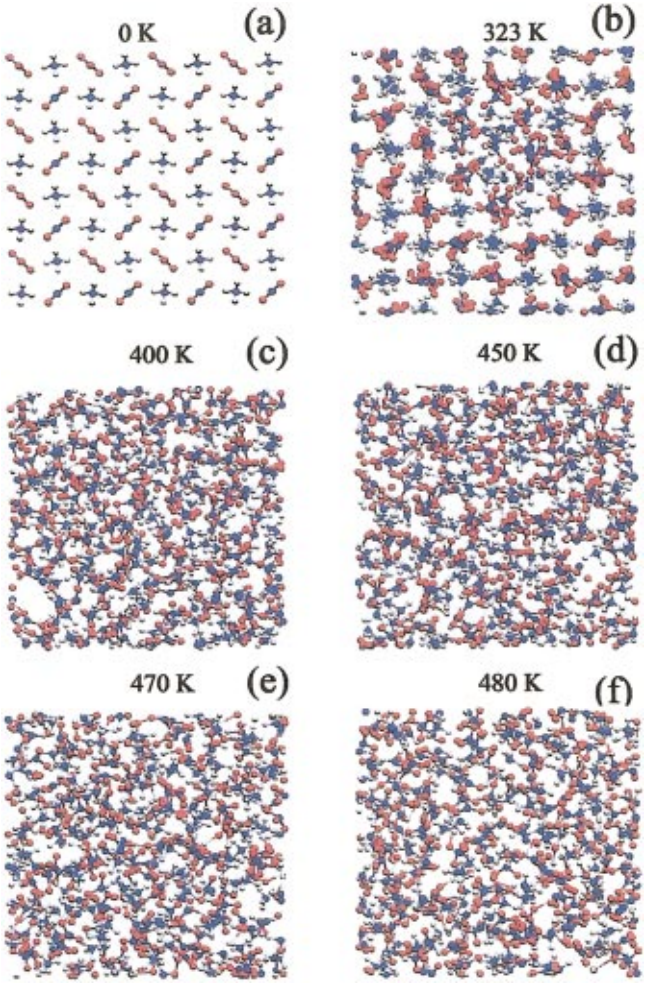

FIG. 4. (Color) The structure of the supercell at various temperatures from simulations with eight molecular voids. The local disorder around the location of the voids is clearly visible. Melting occurs at 475 K.

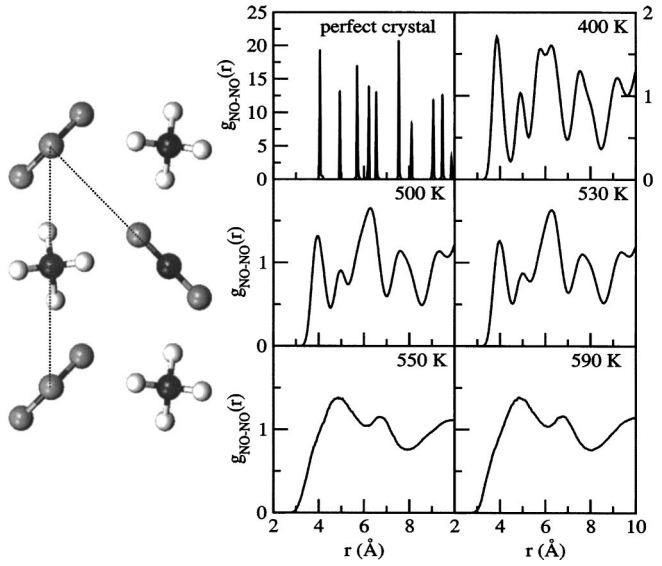

FIG. 5. The RDFs, $g_{\mathrm{NO-NO}}(r)$, for the nitrogen atoms of the nitrate ions for phase-II AN at various temperatures. A section of the phase-II lattice along with two of the nearest neighbor N–N bond distances in the nitrate ions are shown for reference. The colors of the atoms are: dark gray, N; light gray, O; white, H.

sixteen voids, which is in excellent agreement with the experimental melting point of 442 K.

The formation of the local regions of liquidlike structure near voids in the solid is illustrated in Fig. 4, which shows snapshots from simulations at various temperatures for a supercell with eight voids. The liquidlike regions near the voids lower the free energy barrier to the formation of the solid–liquid interface, thus reducing the superheating effect and the calculated melting point. The snapshots of the simulations shown in Fig. 4 along with the density–temperature plots in Fig. 3 show that a solid supercell with eight voids (□) melts in the range 460–500 K.

The RDF for the simulations with no voids can be used to verify that the melting point coincides with the temperature at which the density drop begins, i.e., 540 K. We have calculated the RDF, $g(r)$, for the ammonium–ammonium nitrogen atom pairs (NH–NH) and nitrate–nitrate nitrogen pairs (NO–NO). The RDF is defined as

$$g(r)=\frac{1}{nN}\left\langle \sum_i \sum_j \delta[r-r_{ij}] \right\rangle, \tag{3}$$

where N is the total number of ion pairs, n is the number density, r_{ij} is the distance between nitrogen atoms in nitrates i and j or ammoniums i and j, and the brackets indicate an ensemble average.[32,36] The RDF provides a measure of overall translational structural in the crystal as the temperature varies. The RDFs for the NO–NO pairs at various temperatures and the first two nearest-neighbor distances are shown in Fig. 5. The sharp peaks in the RDF for the perfect phase-II crystal indicate long-range translational correlations in the solid phase. At 400 K vibrational motions broaden the peaks in the RDF relative to those for the perfect crystal, but the locations of the peaks are not shifted. Similar structure in the RDFs is seen for temperatures below 550 K. For example, the maximum of the first peak for temperatures below 550 K is at ~4.0 Å. At 550 K the structure of the RDF undergoes a qualitative change and the maximum of the first peak is shifted to ~4.6 Å. Long-range spatial correlations are destroyed. The RDFs indicate that the melting point is between 530 K and 550 K. The RDF curves for NH–NH pairs at various temperatures are shown in Fig. 6. These RDF curves predict the same melting temperature as those given in Fig. 5.

The density, diffusion coefficient, and viscosity as functions of the temperature were directly determined from MD simulations of liquid AN. Figure 7(a) shows the calculated values of the liquid density as a function of temperature over the range 442–463 K. Experimental data for the density in this narrow stability range for liquid AN are given by Booth and Vinyard.[37] The experimental values of the density were fit to the linear equation[37] $\rho(T)=1.694-6.02\times10^{-4}\,T$ (within 95% confidence limit), which is shown in Fig. 7(a) by the dashed line. The temperature dependence of the calculated liquid-state densities is shown in Fig. 7(a), with error bars that show the root-mean-square deviations of the density over the duration of the simulation. The calculated densities are fit by the linear form $\rho(T)=1.71-6.75\times10^{-4}\,T$, which is shown in Fig. 7(a) by the solid line. From a com-

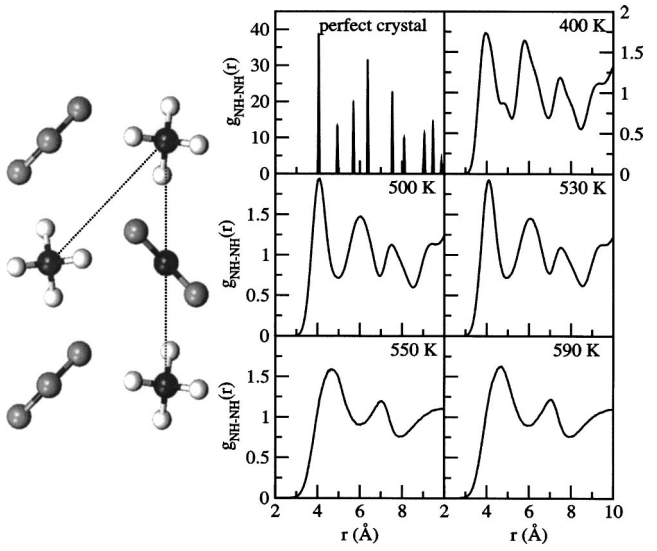

FIG. 6. The RDF for the nitrogen atoms of the ammonium ions, $g_{\mathrm{NH-NH}}(r)$, for phase-II AN at various temperatures. A section of the phase-II lattice along with two of the nearest neighbor N–N bond distances in the ammonium ions are shown for reference. The analysis is similar to that of Fig. 5.

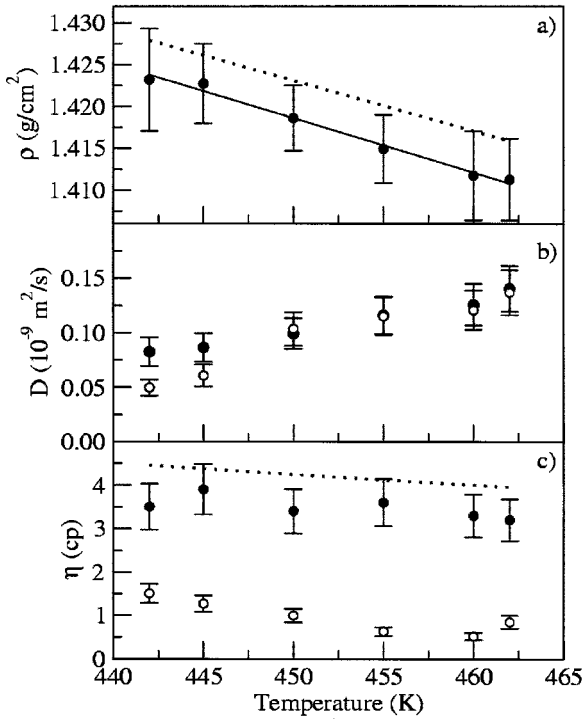

FIG. 7. (a) The calculated density of AN from direct liquid-state calculations. The simulations were done in the temperature range 442–465 K at 1 atm pressure. The slope of the linear fit of the calculated points (—) is in good agreement with the experimental correlation (95% confidence limit) of Booth and Vinyard (Ref. 37) (···). (b) The calculated diffusion coefficients, *D*, for the ammonium (●) and nitrate ions (○) in liquid AN along with corresponding error bars from MD simulations. (c) The calculated liquid viscosity for (●) ammonium and (○) nitrate groups at different temperatures along with corresponding error bars. The dashed line is the experimental result (95% confidence limit) of Booth and Vinyard, Ref. 37.

parison of the slopes of the solid and dashed lines, the temperature dependence of the experimental and calculated results are in good agreement; thus the force field accurately predicts the isobaric compressibility of the liquid. However, the calculated densities are systematically lower than the experimental values. The calculated liquid-state densities are compared to the solid-state densities in Fig. 3.

The temperature dependences of the self-diffusion coefficient of the ammonium (●) and nitrate (○) ions in liquid AN are shown in Fig. 7(b). The self-diffusion coefficient *D* for the ammonium and nitrate ions are calculated from the standard Green–Kubo expression,[36] using the locations of the nitrogen atoms, which correspond to the centers-of-mass of the ions. The nitrate ions have slightly larger self-diffusion coefficients. The temperature dependence of *D* in the range between 442–465 K can be fit to the Arrhenius form[38] $D = A\exp(-E_D/kT)$, where *A* is the pre-exponential factor and E_D is related to the energy barrier to diffusion. The values of *A* and E_D are, respectively, $(1.5\pm0.5)\times10^{-5}$ m^2/s and (45 ± 3) kJ/mol for the ammonium ions and $(18\pm6)\times10^{-5}$ m^2/s and (54 ± 5) kJ/mol for the nitrate ions. The relative error for each of the calculated points is relatively high, on the order of 15%.

We calculated the shear viscosity for the centers of mass of the ammonium and nitrate ions from the general time-correlation function expression.[36,39] In the calculations the mass of each ion was assumed to be located at its center of mass, which corresponds to the position of the nitrogen atom. The viscosities of NH_4^+ and NO_3^- as functions of the temperature over the range 442–463 K are shown in Fig. 7(c). The viscosity of the ammonium (●) and the nitrate (○) ions are both below the experimental viscosity,[37] which is shown by the solid line. The relative error for each of the calculated points is relatively high, on the order of 15%.

IV. ORIENTATIONAL DISORDER IN SOLID AN

In higher temperature simulations of phase II, changes in the solid structure that correspond to the II→I crystalline phase transition are observed. Some of the features of these phases are illustrated in Fig. 1 and were discussed in the Introduction. In phase II the ammonium ions have rotational freedom while the nitrate ions are orientationally disordered between two types of sites, but not rotationally free. The nitrate ions are arranged in parallel rows with planes that are perpendicularly oriented with respect to one another (see Fig. 1). Our simulations show [see Fig. 2(b)] that at 350 K the nitrate ions retain their initial general orientations, but undergo librational motions about their equilibrium orientations.

The rotational orientations of the ammonium and nitrate ions can be quantitatively analyzed by determining ensemble averages of the angle between unit vectors in the direction of the N–O or N–H bonds on different molecules. For this purpose, we have chosen the angles between the two N–O1 bonds in the unit cell that are initially oriented parallel to the *c* axis, that is, we calculated

$$\langle\cos\theta\rangle = \frac{2}{N(N-1)}\sum_{i=1}^{N-1}\sum_{j=i+1}^{N}\mathbf{r}_{\mathrm{NO},i}\cdot\mathbf{r}_{\mathrm{NO},j}\,, \tag{4}$$

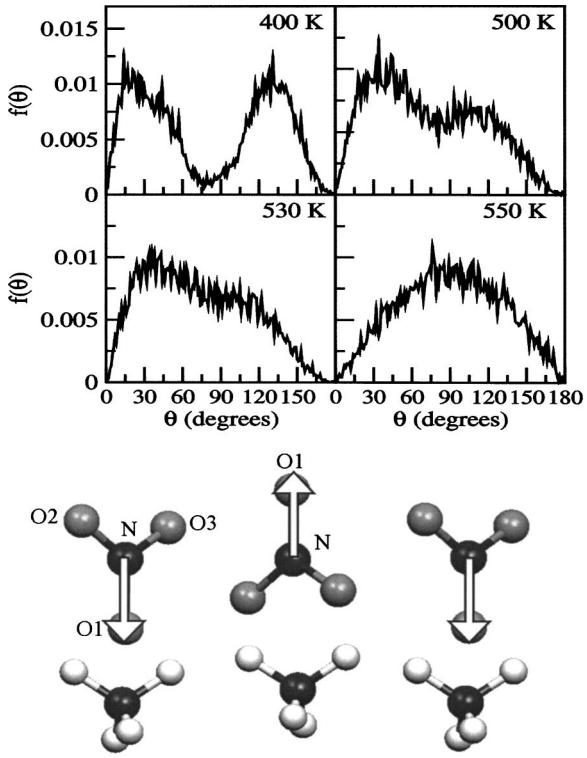

FIG. 8. Dipole–dipole probability distribution $f(\Theta)$ for N–O1 bonds of nitrate ions at various temperatures. The vectors representing the N–O1 bonds are shown for reference. In the perfect crystal, these bonds have equilibrium angles of 0° and 180° with all corresponding vectors in the lattice. The definition of the N–O1 bonds is given along with a fragment of the unit cell.

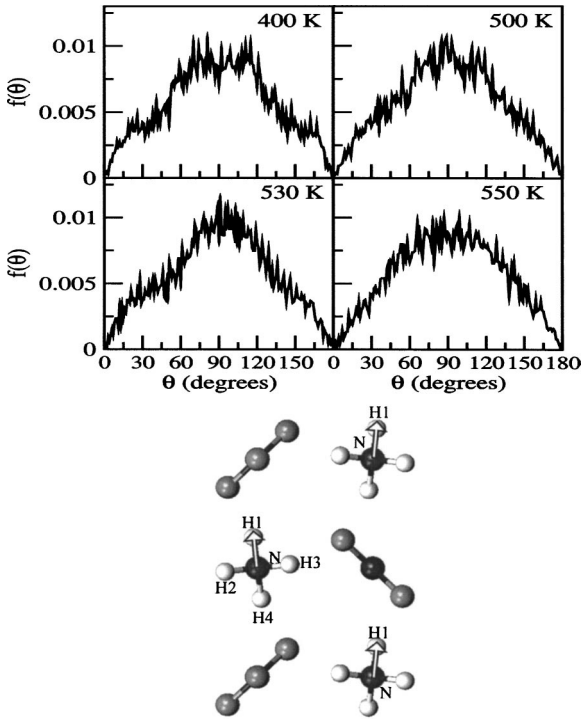

FIG. 9. Dipole–dipole probability distribution $f(\Theta)$ for N–H1 bonds of ammonium ions at various temperatures. The vectors representing the N–H1 bonds are shown for reference. In the perfect crystal, the angles between the N–H1 bonds have equilibrium angles of 0° and 14°. By 400 K, the relative orientations of these vectors have been randomized.

where $\mathbf{r}_{\mathrm{N-O},i}$ is the unit vector in the direction of the N–O1 bond of nitrate ion i which is originally oriented in the direction of the c unit vector. The N–O1 bonds are shown in Fig. 8. Similar calculations can be carried out on the other N–O bonds of the nitrate. A similar definition can be used for the relative orientation of chosen N–H bonds of the ammonium groups, that is,

$$\langle \cos\theta \rangle = \frac{2}{N(N-1)} \sum_{i=1}^{N-1} \sum_{j=i+1}^{N} \mathbf{r}_{\mathrm{NH},i} \cdot \mathbf{r}_{\mathrm{NH},j}, \tag{5}$$

where in this case the N–H1 vectors shown in Fig. 9 are used for reference. The vectors defining the two θ angles are shown on the molecules in Figs. 8 and 9. As seen in Fig. 8, in the perfect crystal the θ angles between the NO1–NO1 vectors are either 0° or 180°. Thermal motions give values for the angles that are centered on the perfect crystal values. The probability distribution $f(\theta)$ is defined as,

$$f(\theta) = \langle \cos\theta \rangle \sin\theta. \tag{6}$$

At 400 K, the most probable angles in the probability distribution $f(\theta)$ between the NO1–NO1 bonds are ~20° and ~130° (see Fig. 8). There is a large barrier to rotation between these two states. As the temperature increases, the most probable angles are shifted and the barrier between the two states decreases. By 530 K, there is a barrierless, almost-free rotation of the NO_3^- groups. After melting, the N–O1 bonds are randomly oriented and the probability of the angular distribution takes the form of a sine curve. The orientations of the N–H1 bonds are almost randomly distributed, even at 400 K. The probability distribution $f(\theta)$ has the form of a sine curve, with some superimposed remnant structure. The original θ values between the chosen N–H1 bonds in the perfect crystal is either 0° (next nearest neighbor ammonium ions) or ~14° (nearest neighbor ammonium ions); see Fig. 9.

The II→I phase transition involves a change from tetragonal to cubic unit cell symmetry with corresponding changes in the unit cell dimensions; $a=5.7193$ Å and $c=4.9326$ Å in phase II to $a=4.3655$ Å in phase I. Along with these changes, the minimum N–N distance for both the nitrate and ammonium ions change from 4.0442 Å in phase-II to 4.3655 Å in phase-I. The RDFs for 530 K in Figs. 5 and 6, however, do not show this change in the N–N distances. A shift of 0.3 Å in the location of the first peak of the RDF would be noticeable on the scale of these two figures. Thus, our model potential correctly predicts the transition to a rotationally free state of the ions in the solid prior to melting (which occurs in phase I), but not the proper relaxation of the ions in the unit cell. We believe this is due to the inaccuracy in the model intermolecular potential we have used, particularly, the description of hydrogen bonding. The typical strong directionality of hydrogen bonding is not reflected in the form chosen for $V^{\mathrm{HB}}(r)$ used in Eq. (2). The major focus of our interest in this study was the prediction of the melting transition, not crystalline phase transitions, and for the sake of wider applications of our approach we were interested in showing that melting point is accurately predicted with a relatively simple potential. But, we believe that it is worth stressing here that this simple potential also quali-

tatively describes the II→I phase transition. This result suggests that giving more attention to the details of the interactions in the formulation of a potential for AN, and of course more appropriate simulations, this crystalline phase transition could be accurately simulated. Likewise, even the more complicated phase transitions in ionic solids could be modeled.

In this simulation, the symmetry imposed on the supercell is expected to have a minor effect on the solid-state phase transition. The constraint of isotropic volume variations on the supercell in the NPT simulations prevents changes in the supercell shape. However, we do not believe that this is a significant factor in the II→I phase transition, which involves a change from a tetragonal to a cubic unit cell. The changes in the positions of the ions in the II→I phase transition is not large. The ions undergo fairly small amplitude motions and retain the basic perpendicular structure of the unit cell vectors. Thus, the symmetry constraints imposed in the NPT simulation are not expected to be an important factor. Rotational freedom of the nitrate ions does not require the displacement of the centers-of-mass of the ions within the unit cell and should not be strongly affected by the large-scale symmetry constraints imposed on the supercell in this simulation.

Another factor that needs to be considered is superheating.[17,34] We observe the change in the rotational freedom of the nitrate ions at a higher temperature (~530 K; 20 K below the calculated melting point) than is observed experimentally (398 K; 44 K below the experimental melting point). The fact that the ions begin to gain rotational freedom at a temperature higher than experiment may in large part be due to an anomalously high Gibbs free energy barrier separating the phases, which is very likely due the inaccuracy of the potential.

The main point we have established is that the melting transition can be accurately predicted in simulations initiated at a crystal phase lower in energy than the one in equilibrium with the liquid phase and, significantly, the crystalline phase transition can be qualitatively predicted with a relatively simple interaction potential. The importance of being able to accurately predict melting points is obvious. The results for the crystalline phase transition are encouraging. They indicate that with a more accurate potential used in simulations designed to obviate the superheating effect and allow for the minor symmetry change, the crystalline phase transition can be accurately modeled.

V. SUMMARY AND CONCLUSIONS

The melting point and liquid-state properties of AN were determined by MD simulations of $4\times4\times5$ supercells, which comprises 160 ion pairs. The force field used in these simulations is that developed by Sorescu and Thompson.[13] The determination of the melting point was based on the variation of the density, and RDF. The calculated melting point from direct simulations of the $4\times4\times5$ supercell with voids to eliminate superheating effects in the solid is in the range 442–445 K, which is in excellent agreement with the experimental value of 442 K. The simulations also describe some features of the II→I crystalline phase change. The results for the II→I crystalline phase change are encouraging. The results suggest that with some improvements in the potential and by using a more sophisticated simulation method to allow for the overall structural changes and to obviate the superheating effect, the crystalline phase change could be accurately simulated.

ACKNOWLEDGMENTS

The authors are grateful to Dr. Paras M. Agrawal for several fruitful discussions. We are also grateful to Dr. Donald R. Thomas of the Mississippi Chemical Corporation for beneficial communications.

[1] A compilation of physical constants for ammonium nitrate along with literature references may be found at: http://www.angelfire.com/ms/dthomaschemist/
[2] C. S. Choi and H. J. Prask, Acta Crystallogr., Sect. B: Struct. Sci. **B39**, 414 (1983).
[3] M. Ahtee, K. J. Smolander, B. W. Lucas, and A. W. Hewat, Acta Crystallogr., Sect. C: Cryst. Struct. Commun. **C39**, 651 (1983).
[4] T. M. Lowry and F. C. Hemmings, J. Soc. Chem. Ind. (Lond.) **39**, 101 (1920).
[5] J. R. Hoden and C. W. Dickinson, J. Phys. Chem. **79**, 249 (1975).
[6] C. S. Choi, J. E. Maples, and E. Prince, Acta Crystallogr., Sect. B: Struct. Crystallogr. Cryst. Chem. **B28**, 1357 (1972).
[7] B. W. Lucas, M. Ahtee, and A. W. Hewat, Acta Crystallogr., Sect. B: Struct. Crystallogr. Cryst. Chem. **B35**, 1038 (1979).
[8] R. N. Brown and A. C. McLaren, Proc. R. Soc. London, Ser. A **266**, 329 (1962).
[9] M. Ahtee, K. Kurki-Suonio, B. W. Lucas, and A. W. Hewat, Acta Crystallogr., Sect. A: Cryst. Phys., Diffr., Theor. Gen. Crystallogr. **A35**, 591 (1979).
[10] S. Yamamoto and Y. J. Shinnaka, J. Phys. Soc. Jpn. **37**, 724 (1974).
[11] K. Østerlund and H. J. Rosen, Solid State Commun. **15**, 1355 (1974).
[12] N. G. Parsonage and L. A. K. Staveley, *Disorder in Crystals* (Oxford University Press, Oxford, 1978).
[13] D. C. Sorescu and D. L. Thompson, J. Phys. Chem. A **105**, 720 (2001).
[14] M. L. Klein, *Molecular Dynamics Simulations of Statistical Mechanical Systems*, edited by G. Ciccotti and W. G. Hoover (North–Holland, Amsterdam, 1986), p. 424; M. L. Klein, I. R. McDonald, and Y. Ozaki, J. Chem. Phys. **79**, 5579 (1983); R. J. C. Brown and R. M. Lynden-Bell, J. Phys.: Condens. Matter **6**, 9903 (1994); B. Guillot and T. Guissani, J. Chem. Phys. **116**, 2047 (2002).
[15] M. de Koning, A. Antonelli, and S. Yip, J. Chem. Phys. **115**, 11025 (2001).
[16] J. G. Dash, Rev. Mod. Phys. **71**, 1737 (1999).
[17] K. Lu and Y. Li, Phys. Rev. Lett. **80**, 4474 (1998).
[18] L. Zhang, Z. H. Jin, L. H. Zhang, M. L. Sui, and K. Lu, Phys. Rev. Lett. **85**, 1484 (2000).
[19] S. R. Phillpot, J. F. Lutsko, D. Wolf, and S. Yip, Phys. Rev. B **40**, 2831 (1989).
[20] J. F. Lutsko, D. Wolf, S. R. Phillpot, and S. Yip, Phys. Rev. B **40**, 2841 (1989).
[21] J. Solca, A. J. Dyson, G. Steinebrunner, B. Kirchner, and H. Huber, J. Chem. Phys. **108**, 4107 (1998).
[22] P. M. Agrawal, B. M. Rice, and D. L. Thompson, J. Chem. Phys. **119**, 9617 (2003).
[23] G. F. Velardez, S. Alavi, and D. L. Thompson, J. Chem. Phys. **119**, 6698 (2003).
[24] C. M. Breneman and K. B. Wiberg, J. Comput. Chem. **11**, 361 (1990).
[25] C. Bayly, P. Cieplak, W. D. Cornell, and P. A. Kollman, J. Phys. Chem. **97**, 10269 (1993).
[26] D. A. Case *et al.*, AMBER 7 (University of California, San Francisco, 2002).
[27] W. D. Cornell, P. Cieplak, C. L. Bayly, I. R. Gould, K. M. Merz Jr., D. M. Ferguson, D. C. Spellmeyer, T. Fox, J. W. Caldwell, and P. A. Kollman, J. Am. Chem. Soc. **117**, 5179 (1995).
[28] D. C. Sorescu and D. L. Thompson, J. Phys. Chem. B **103**, 6774 (1999).
[29] T. R. Forester and W. Smith, DL POLY 2.12 (CCLRC, Daresbury Laboratory, Daresbury, England, 1995).

[30] S. Nosé, J. Chem. Phys. **81**, 511 (1984).
[31] W. G. Hoover, Phys. Rev. A **31**, 1695 (1985).
[32] M. P. Allen and D. J. Tildesley, *Computer Simulation of Liquids* (Oxford Science Publications, Oxford, 1987).
[33] K. D. Gibson and H. A. Scheraga, J. Phys. Chem. **99**, 3752 (1995).
[34] S.-N. Luo and T. J. Ahrens, Appl. Phys. Lett. **82**, 1836 (2003); S.-N. Luo, T. J. Ahrens, T. Çağin, A. Strachan, W. A. Goddard III, and D. C. Swift, Phys. Rev. B **68**, 134206 (2003).
[35] P. M. Agrawal, B. M. Rice, and D. L. Thompson, J. Chem. Phys. **118**, 9680 (2003).
[36] D. A. McQuarrie, *Statistical Mechanics* (Harper & Row, New York, 1976).
[37] D. H. Booth and V. C. Vinyard, J. Appl. Chem. **17**, 86 (1967).
[38] J. M. Haile, *Molecular Dynamics Simulation: Elementary Methods* (Wiley, New York, 1992).
[39] M. Schoen and C. Hoheisel, Mol. Phys. **56**, 653 (1985).